

Quantum Oscillations in a Topological Insulator $\text{Bi}_2\text{Te}_2\text{Se}$ with Large Bulk Resistivity ($6 \Omega\text{cm}$)

Jun Xiong¹, A. C. Petersen^{1,2}, Dongxia Qu¹, R. J. Cava² and N. P. Ong¹

¹*Department of Physics and* ²*Department of Chemistry, Princeton University, New Jersey 08544, U.S.A.*
(Dated: November 21, 2018)

We report the observation of prominent Shubnikov-de Haas oscillations in a Topological Insulator, $\text{Bi}_2\text{Te}_2\text{Se}$, with large bulk resistivity ($6 \Omega\text{cm}$ at 4 K). By fitting the SdH oscillations, we infer a large metallicity parameter $k_F\ell = 41$, with a surface mobility ($\mu_s \sim 2,800 \text{ cm}^2/\text{Vs}$) much larger than the bulk mobility ($\mu_b \sim 50 \text{ cm}^2/\text{Vs}$). The plot of the index fields B_ν vs. filling factor ν shows a $\frac{1}{2}$ -shift, consistent with massless, Dirac states. Evidence for fractional-filling states is seen in an 11-T field.

Topological Insulators are predicted to bear current-carrying, massless, Dirac surface states that traverse the bulk energy gap [1–4]. These unusual surface states have been observed by angle-resolved photoemission spectroscopy (ARPES) [5–8] and scanning tunneling microscopy experiments (STM) [9]. Quantization of the Dirac states into Landau Levels has been demonstrated in STM experiments [10, 11]. Observation of the surface currents by transport has been more challenging [12, 13]. Recently, however, encouraging progress has been achieved. The surface SdH oscillations and surface mobility was measured in Bi_2Te_3 crystals [14]. The existence of surface states at fractional filling in a pulsed magnetic field were reported in $(\text{Bi,Sb})\text{Se}_3$ [15]. Here we report the observation of prominent SdH oscillations in crystals of $\text{Bi}_2\text{Te}_2\text{Se}$ with very large bulk resistivity. Evidence for fractional-filling states become apparent at relatively low magnetic fields.

Recently, ARPES experiments have shown that $\text{Bi}_2\text{Te}_2\text{Se}$ displays a single topological surface state [16]. Independent of our experiment, SdH oscillations in this compound have also been reported by Y. Ando's group [17]. We were motivated to grow crystals of $\text{Bi}_2\text{Te}_2\text{Se}$ by reasoning that Bi_2Se_3 crystals grow with a stable density of Se vacancies. Electrons donated by the vacancies pin the Fermi energy E_F to the conduction band, resulting in a negative thermopower S at low temperature T . By contrast, as-grown Bi_2Te_3 typically has a positive thermopower. By growing a series of the hybrid semiconductor $\text{Bi}_2\text{Se}_{1+x}\text{Te}_{2-x}$, we have found that the low-temperature thermopower varies systematically, reflecting changes in E_F . Crystals were grown by a modified Bridgeman method from high purity elemental starting materials. After heating for one day at 850 C in a clean evacuated quartz tube, the melt was cooled in a temperature gradient to 500 C where it was left to anneal for 2 days before cooling rapidly to room temperature. For the composition $\text{Bi}_2\text{Te}_2\text{Se}$, S rises to very large values. With a razor blade, we cleaved thin crystals and attached contacts using silver paint. For the sample here, the crystal thickness $d = 110 \mu\text{m}$, while the distance between voltage leads equals 0.5 mm. The resistivity profile measured at $B = 0$ is shown in Fig. 1a. Below 40 K, the value of ρ attains values in the range 5–6 Ωcm , or ~ 1000 times higher than in non-metallic Bi_2Te_3 . Expressed as

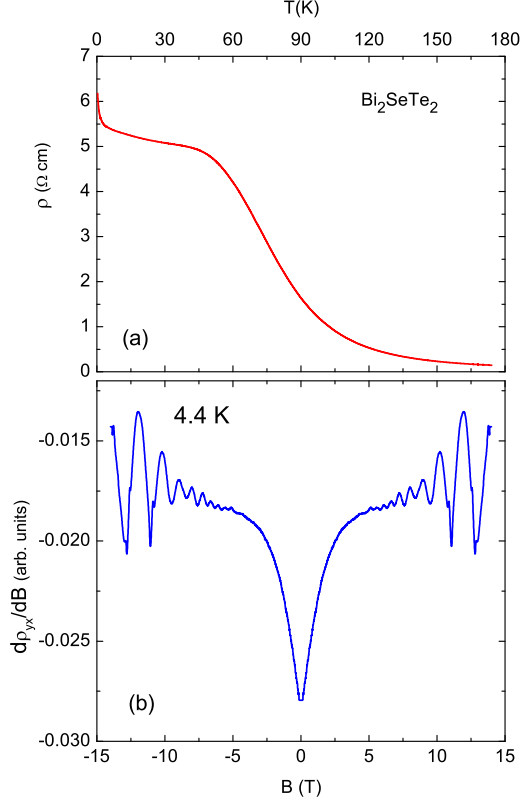


FIG. 1: (Color online) The resistivity of a cleaved crystal of the Topological Insulator $\text{Bi}_2\text{Te}_2\text{Se}$. Panel (a) shows ρ vs. T measured in $B = 0$. Below 10 K, ρ attains the value $5.5 \Omega\text{cm}$, or an areal resistance $R_\square = 400 \Omega$. Despite the non-metallic value of R_\square , sizeable quantum oscillations are observed below 38 K. Panel (b) displays the prominent SdH oscillations observed in the derivative $d\rho_{xy}/dB$ vs. B at 4.4 K.

an areal resistance $R_\square = \rho/d$, the low- T resistance corresponds to $R_\square = 400 \Omega$. Despite the high resistance, ρ is only weakly T -dependent, displaying a $\log T$ increase as $T \rightarrow 0$. The observed Hall coefficient R_H below 10 K (n -type) implies a very small bulk carrier concentration $n_b \sim 2.6 \times 10^{16} \text{ cm}^{-3}$. Combining this with the observed

ρ , we infer a low bulk mobility $\mu_b \sim 50 \text{ cm}^2/\text{Vs}$.

Such a low μ_b should not produce SdH oscillations for $B < 14 \text{ T}$. Surprisingly, however, the Hall resistivity ρ_{yx} displays prominent SdH oscillations that may be resolved up to 40 K. To date, we have detected SdH oscillations in 4 crystals of $\text{Bi}_2\text{Te}_2\text{Se}$ with ρ - T profiles similar to that in Fig. 1a. Figure 1b shows the trace of the derivative $d\rho_{yx}/dT$ vs. B at $T = 4.4 \text{ K}$. Independently, SdH oscillations were also observed in $\text{Bi}_2\text{Te}_2\text{Se}$ by Y. Ando *et al.* [17].

The surface conductance and bulk conductance act as parallel channels for charge transport. The observed conductivity σ_{ij} is then the sum

$$\sigma_{ij} = \sigma_{ij}^b + G_{ij}^s/d, \quad (1)$$

where σ_{ij}^b is the bulk conductivity and G_{ij}^s the conductance matrix of the surface states. To exploit the additivity, we have converted the measured resistivity matrix ρ_{ij} to the conductivity matrix σ_{ij} . To amplify the surface contribution to σ_{xy} , we define $\Delta\sigma_{xy} = \sigma_{xy} - \langle\sigma_{xy}\rangle$ where $\langle\sigma_{xy}\rangle$ is a smoothed background.

Figure 2 displays the subtracted quantity $\Delta\sigma_{xy}$ versus $1/B$ over the temperature interval $0.3 < T < 38 \text{ K}$. With increasing T , the amplitude of the SdH oscillations decreases rapidly as T increases above 10 K.

To analyze the SdH oscillations, we have fitted the curves using the standard expression [18]

$$\frac{\Delta\sigma_{xy}}{\sigma_{xy}} = \left(\frac{\hbar\omega_c}{2E_F}\right)^{\frac{1}{2}} \frac{\lambda}{\sinh\lambda} e^{-\lambda_D} \cos\left[\frac{2\pi E_F}{\hbar\omega_c} + \frac{\pi}{4}\right], \quad (2)$$

with $\lambda = 2\pi^2 k_B T / \hbar\omega_c$ and $\lambda_D = 2\pi^2 k_B T_D / \hbar\omega_c$, where ω_c is the cyclotron frequency and the Dingle temperature is given by $T_D = \hbar / (2\pi k_B \tau)$, with τ the lifetime. Compared with the SdH expression for the conductivity σ_{xx} , the phase ϕ in the Hall conductivity is shifted by $\pi/2$ ($-\pi/4 \rightarrow \pi/4$). For 2D systems, we may write the SdH frequency as $2\pi E_F B / (\hbar\omega_c)$, which simplifies to $4\pi^2 \hbar n_s / e$, with the 2D carrier density $n_s = k_F^2 / 4\pi$ (per spin). As shown in Ref. [19], Eq. 2 may be employed in a Dirac system if we write the cyclotron mass as $m_c = E / v_F^2$.

We have found that the oscillations cannot be fitted using one SdH frequency. For $T < 6 \text{ K}$, the sharp decrease of the oscillation amplitude for $B^{-1} > 0.12 \text{ T}^{-1}$ suggests beating between 2 terms of nearly equal frequencies. Indeed, a good fit is obtained if we add a second term identical to the one in Eq. 2 except for a slight difference in n_s . The measured curve of $\Delta\sigma_{xy}$ was fitted with the 2 terms (the absolute value of the surface Hall conductance G_{xy} is not known). There are altogether 5 adjustable parameters (n_{si} and amplitude A_i , with $i = 1, 2$) and T_D (assumed same for both). The best fit (Fig. 3a) is obtained with $A_1 = A_2$ and densities differing by only 5% [$(n_{s1}, n_{s2}) = (1.79, 1.71) \times 10^{12} \text{ cm}^{-2}$], corresponding to an average Fermi wavevector $k_F = 0.047 \text{ \AA}^{-1}$. The fit yields $T_D = 8.5 \pm 1.5 \text{ K}$, which corresponds

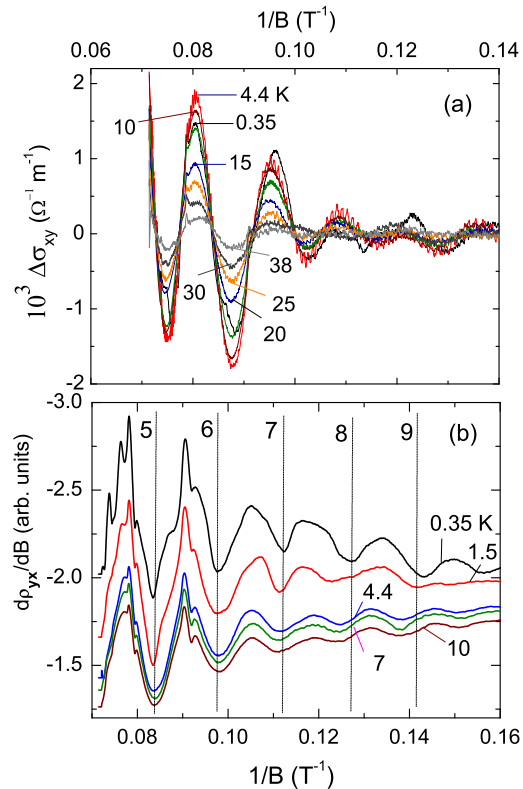


FIG. 2: (Color online) The Hall SdH oscillations versus $1/B$ at selected T . In Panel (a), we have plotted the subtracted Hall conductivity $\Delta\sigma_{xy}$ to highlight the decrease of the amplitude over 2 decades in T (0.3 to 38 K). Panel (b) displays traces of the Hall resistivity $d\rho_{yx}/dB$ at 5 temperatures. The minima in $|d\rho_{yx}/dB|$ are used to fix the index field B_ν (dashed lines with ν indicated). For LL with $\nu < 6$, sharp structures are observed between integer filling.

to a mean-free-path $\ell = 70\text{-}100 \text{ nm}$ and a surface mobility $\mu_s = e\ell/\hbar k_F = 2,800 \pm 250 \text{ cm}^2/\text{Vs}$. Interestingly, μ_s is strongly enhanced over μ_b (by ~ 60).

By fitting to the decrease in amplitude with T at fixed B (12.4 T), we obtain an effective mass $m^* = 0.089 m_e$. Together with k_F , we obtain a Fermi velocity $v_F \sim 6 \times 10^5 \text{ m/s}$, higher than that in Bi_2Te_3 .

The high mobility provides strong evidence that the SdH oscillations arise from surface states. Suppose for the sake of argument that the oscillations come from bulk states. The SdH period must then be identified with a 3D Fermi sphere of radius $k_F = 0.047 \text{ \AA}^{-1}$, or a 3D density of $3.3 \times 10^{18} \text{ cm}^{-3}$. The inferred μ then implies a 3D resistivity $\rho_b \sim 0.7 \text{ m}\Omega\text{cm}$ at 4.4 K. The large discrepancy (factor of 9,000) from the observed value argues firmly against a bulk origin.

Hence we conclude that the SdH oscillations come from high mobility surface carriers. The two periods

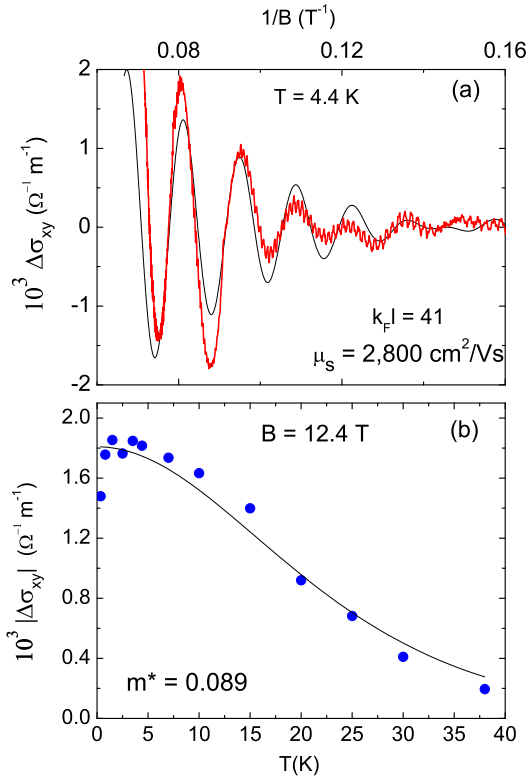


FIG. 3: (Color online) Fits of $\Delta\sigma_{xy}$ to extract mobility. Panel (a) shows the fit to $\Delta\sigma_{xy}$ at $T = 4.4$ K to Eq. 2. The rapid decrease of the oscillation amplitude for $1/B > 0.09$ T^{-1} reflects interference between 2 terms of equal amplitudes and densities $(n_{s1}, n_{s2}) = (1.8, 1.7) \times 10^{12}$ cm^{-2} . The fit yields mobility $\mu = 2,800$ cm^2/Vs , and $k_F\ell = 41$. Panel (b) shows the fit of the envelope versus T with B fixed at 12 T. The fit yields $m^* = 0.089$ m_0 (free mass). With $k_F = 0.047$ \AA^{-1} , the inferred velocity $v_F = 6 \times 10^5$ m/s.

likely arise from the large surfaces of the cleaved crystal that are normal to \mathbf{B} . From the inferred n_{s1} and μ , we find that the conductance of each surface is $G_s = \frac{1}{2}(e^2/h)k_F\ell \simeq 0.72$ mS (or $R_{\square} \sim 1.39$ k Ω).

The prominence of the oscillations allows us to address the question whether the surface states have a Dirac dispersion. In principle, one may plot the “index” field $1/B_\nu$ versus the integers $\nu = 1, 2, \dots$, and track the intercept in the limit $B \rightarrow \infty$. However, away from the quantum Hall effect (QHE) regime at low B , it is sometimes uncertain whether one should take the maxima or minima of ρ_{xx} or ρ_{yx} for the index field. To us, the most natural choice is the field defined by the filling factor $\nu \equiv N_e/N_\phi$, viz.

$$B_\nu = n_s\phi_0/\nu, \quad (3)$$

where N_e and N_ϕ are the total number of electrons on a surface and the number of flux quanta $\phi_0 = h/e$ pierc-

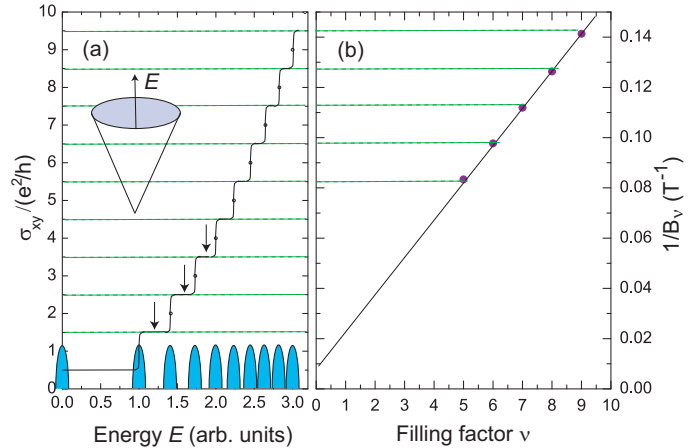


FIG. 4: (Color online) Construction used to fix the filling factor for a Dirac spectrum. Panel (a) sketches schematically the step-like increase of $\sigma_{xy} = (e^2/h)[\nu + \frac{1}{2}]$ versus energy E , where $\frac{1}{2}$ arises from the $\nu = 0$ LL at the Dirac point. The half-ovals are broadened Landau Levels centered at $E_\nu = \hbar\ell_B^{-1}v_F\sqrt{2\nu}$. B_ν are the fields at which ζ falls between LLs (arrows). The inset shows the 2D Dirac energy surface in zero B . In Panel (b), the measured values of $1/B_\nu$ are plotted versus filling factor ν . The 5 values of $1/B_\nu$ fall on a straight line that intercepts the ν axis at -0.55 , consistent with a Dirac spectrum.

ing the surface (hereafter, we focus on one surface, i.e. one spin degree of freedom). Equation 3 is equivalent to having exactly ν flux quanta enclosed in the cyclotron orbit for an electron in the LL ν , viz. $B\pi k_F^2\ell_B^4 = \nu\phi_0$, where $\ell_B = \sqrt{\hbar/eB}$ is the magnetic length. Hence, the chemical potential ζ lies between 2 LLs when $B = B_\nu$.

To show how the line of $1/B_\nu$ vs. ν relates to the Dirac dispersion, we employ the construction in Fig. 4. In Panel (a), we have sketched the steps of the quantized Hall conductivity $\sigma_{xy} = (e^2/h)(\nu + \frac{1}{2})$ versus energy E , where the important shift of $\frac{1}{2}$ arises from the $\nu = 0$ LL at the Dirac point, as in graphene. The half-ovals drawn on the E -axis represent the broadened LLs. As the peaks occur at the step-edges of σ_{xy} , they also locate the maxima in $d\rho_{yx}/dB$. Consequently, the minima in $|d\rho_{yx}/dB|$ locate B_ν , the field at which ζ lies between LLs (arrows). The $\frac{1}{2}$ -shift means that the line of $1/B_\nu$ vs. ν in Panel (b) does not pass through the origin (unlike the case of a quadratic dispersion).

In Fig. 4b, we have plotted the measured $1/B_\nu$ versus ν . With just one vertical scale adjustment, we can align the 5 data points to the steps in Panel (a). At our highest B , the filling factor is $\nu = 5$. More significantly, the line through the data in (b) intercepts the ν axis at $\nu = -0.55$ instead of 0. Hence our results are consistent with the $\frac{1}{2}$ shift expected from a Dirac spectrum.

Recently, Fisher *et al.* observed fractional-filling states in (Bi,Sb)Se3 in very intense fields (>50 T). In our experiment, evidence for fractional-filling begin to emerge

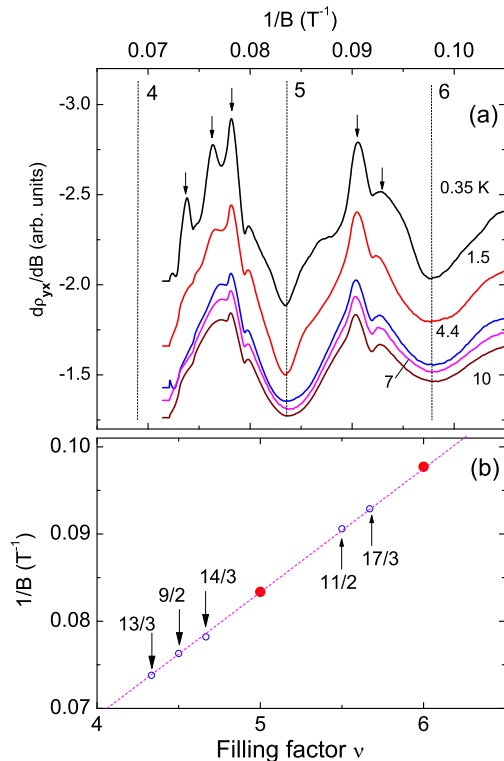


FIG. 5: (Color online) Panel (a): Expanded view of $d\rho_{yx}/dB$ for $4 < \nu < 6$ showing sharp maxima at non-integer values of ν , at T from 0.35–10 K. The arrows locate the more prominent peaks. In Panel (b), the peak positions plotted against ν align well with fractional values of ν (arrows mark the values $\nu = 13/3, 9/2, \dots, 17/3$).

at much lower fields (11 T). As shown in Fig. 5a, an intriguing array of sharp *maxima* in $d\rho_{yx}/dB$ (arrows) is apparent for $4 < \nu < 6$. The peaks become weaker as T increases from 0.35 K, but some are still resolved at 10 K. Interestingly, the peak positions align well with fractional values of ν , as shown in Fig. 5b.

As in the fractional QHE regime in GaAs and graphene, we interpret the peaks as evidence for many-body states that are stabilized at fractional ν . However, there are several puzzling features (when compared with the standard FQHE phenomenology). First, in Fig. 5a, we find that the maxima of $|d\rho_{yx}/dB|$ locate the fractional values of ν whereas B_ν for integer ν is fixed by the minima. We do not have an explanation for this inversion. Second, the fractional-filling peaks are observed at fairly large ν , whereas in GaAs, they are difficult to resolve for $\nu > 2$, despite the much higher μ_s in GaAs. Finally, unlike in GaAs, the fractions corresponding to $\frac{1}{2}$ are more prominent here (particularly 11/2) than those corresponding to $\frac{1}{3}$ or $\frac{2}{3}$. In this system, we may incorporate features such as the linear Dirac dispersion, strong spin-orbit interaction, and strong suppression of $2k_F$ scattering to understand the states at fractional filling.

We acknowledge support from the National Science Foundation under grant DMR 0819860 and from the Nano Electronics Research Corporation (Award 2010-NE-2010G). We thank Liang Fu, Duncan Haldane and Andrei Bernevig for explaining the filling of LLs in the 2D Dirac system.

-
- [1] L. Fu, C. L. Kane, E. J. Mele, Phys. Rev. Lett. **98**, 106803 (2007).
 - [2] L. Fu, C. L. Kane, Phys. Rev. B **76**, 045302 (2007).
 - [3] J. E. Moore, L. Balents, Phys. Rev. B **75**, 121306(R) (2007).
 - [4] B. A. Bernevig, T. Hughes, S. C. Zhang, Science **314**, 1757-1761 (2006).
 - [5] D. Hsieh *et al.*, Nature **452**, 970-974 (2008).
 - [6] D. Hsieh *et al.*, Science **323**, 919-922 (2009).
 - [7] Y. Xia *et al.*, Nature Phys **5**, 398-402 (2009).
 - [8] Y. L. Chen *et al.*, Science **325**, 178-181 (2009).
 - [9] P. Roushan *et al.*, Nature **460**, 1106 (2009)
 - [10] T. Hanaguri, K. Igarashi, M. Kawamura, H. Takagi, and T. Sasagawa, Phys. Rev. B **82**, 081305(R) (2010).
 - [11] Peng Cheng *et al.*, Phys. Rev. Lett. **105**, 076801 (2010).
 - [12] J. G. Checkelsky *et al.*, Phys. Rev. Lett. **103**, 246601 (2009).
 - [13] A.A. Taskin, Yoichi Ando, Phys. Rev. B **80**, 085303 (2009).
 - [14] Dong-Xia Qu, Y. S. Hor, Jun Xiong, R. J. Cava and N. P. Ong, Science **329**, 821 (2010).
 - [15] James G. Analytis, Ross D. McDonald, Scott C. Riggs, Jiun-Haw Chu, G. S. Boebinger and Ian R. Fisher, Nature Physics **6**, 960 (2010).
 - [16] M. Z. Hasan, *private communication*.
 - [17] Zhi Ren, A. A. Taskin, Satoshi Sasaki, Kouji Segawa, and Yoichi Ando, Phys. Rev. B **82**, 241306(R) (2010). Ando's group and our group announced the SdH results observed in this compound at the workshop on Topological Insulators & Superconductors, Princeton, Nov. 3-5, 2010.
 - [18] See for e.g., Bharat Jalan, Susanne Stemmer, Shawn Mack and S. James Allen, Phys. Rev. B **82**, 081103 (2010).
 - [19] V. P. Gusynin and S. G. Sharapov, Phys. Rev. B **71**, 125124 (2005).
 - [20] Yuanbo Zhang, Yan-Wen Tan, Horst L. Stormer and Philip Kim, Nature **438**, 201 (2005).